

# Benchmarking 6DOF Urban Visual Localization in Changing Conditions

Torsten Sattler<sup>1</sup> Will Maddern<sup>2</sup> Akihiko Torii<sup>3</sup> Josef Sivic<sup>4,5</sup>  
 Tomas Pajdla<sup>5</sup> Marc Pollefeys<sup>1,6</sup> Masatoshi Okutomi<sup>3</sup>

<sup>1</sup>Department of Computer Science, ETH Zürich  
<sup>2</sup>Oxford Robotics Institute, University of Oxford, UK

<sup>3</sup>Tokyo Institute of Technology <sup>4</sup>Inria\*

<sup>5</sup>CIIRC, Czech Technical University in Prague <sup>6</sup>Microsoft, Redmond

## Abstract

*Visual localization enables autonomous vehicles to navigate in their surroundings and Augmented Reality applications to link virtual to real worlds. In order to be practically relevant, visual localization approaches need to be robust to a wide variety of viewing condition, including day-night changes, as well as weather and seasonal variations. In this paper, we introduce the first benchmark datasets specifically designed for analyzing the impact of such factors on visual localization. Using carefully created ground truth poses for query images taken under a wide variety of conditions, we evaluate the impact of various factors on the quality of 6 degree-of-freedom (6DOF) camera pose estimation through extensive experiments with state-of-the-art localization approaches. Based on our results, we draw conclusions about the difficulty of different conditions and propose promising avenues for future work. We will eventually make our two novel benchmarks publicly available.*

## 1. Introduction

Estimating the 6DOF camera pose of an image with respect to a 3D scene model is key for visual navigation of autonomous vehicles and augmented/mixed reality devices such as Google Tango [25] or Microsoft HoloLens [44]. Solutions to this *visual localization* problem can also be used to “close loops” in the context of SLAM or to register query images to Structure-from-Motion (SfM) reconstructions.

Work on 3D based visual localization has mainly focussed on increasing efficiency [35, 60, 61], including applicability to mobile devices [41], improving scalability by handling ambiguous matches arising from locally similar structures [34, 58, 73, 84], and reducing memory requirements [13, 35, 58]. However, the impact of various viewing

\*WILLOW project, Departement d’Informatique de l’École Normale Supérieure, ENS/INRIA/CNRS UMR 8548, PSL Research University.

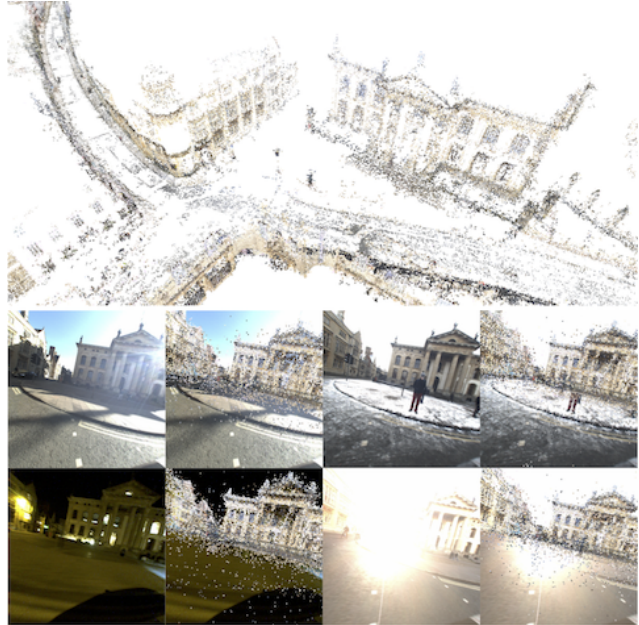


Figure 1. Visual localization in changing urban conditions. We present two new datasets, *Aachen Day-Night* and *RobotCar Seasons* (shown), for evaluating 6DOF localisation against a prior 3D map (top) using registered query images taken from a wide variety of conditions (bottom), including day-night variation, weather and seasonal changes over long periods of time.

and environmental conditions such as day-night or seasonal changes on the localization performance and pose estimation accuracy has received little attention.

Interestingly, the impact of changing conditions on the highly related *place recognition* problem has received significant attention, especially in the robotics community [16, 40, 46, 51, 72, 76] where robust localization under varying conditions is critical for visual navigation of autonomous vehicles. Work on long-term place recognition aims at developing image and feature representations that are stable over time and can thus be used to relate images even under strong appearance changes. However, these representations

are typically not robust to viewpoint changes, and existing benchmarks for long-term place recognition often contain little change in viewpoint. This renders them less useful for benchmarking 6DOF visual localization.

The main goal of this paper is to create a benchmark for analyzing the impact of changing condition on visual localization methods. To this end, we have created two benchmark datasets addressing various tasks: The *Aachen Day-Night* dataset represents a pedestrian scenario were images are taken with a mobile phone cameras, and is focussed on localizing individual images taken during night against a 3D SfM model constructed exclusively from day-time images. The *RobotCar Seasons* dataset considers visual localization for autonomous vehicles in a wide range of viewing conditions (*c.f.* Fig. 1). Besides localizing individual images, we also consider the impact of using multi-camera systems and short sequences of photos on the localization performance.

**Contributions.** This paper makes the following contributions: (i) we create a new outdoor benchmark complete with ground truth and metrics for evaluating 6DOF visual localization under changing conditions such as illumination (day/night), weather (sunny/rain/snow), and seasons (summer/winter) and (ii) our benchmark covers multiple scenarios, such as pedestrian and vehicle localization, and localization from single and multiple images as well as sequences. We evaluate multiple state-of-the-art algorithms for each use-case. (iii) an extensive experimental evaluation provides interesting insights into the difficulty of different conditions. Especially, we are able to determine the relative challenge of different weather and illumination conditions, and how useful multi-camera systems are for localization. (iv) based on our experimental results, we point out interesting avenues for future research on visual localization. (v) we will eventually make our benchmark publicly available.

We hope that the datasets proposed in this paper will stimulate research on visual localization methods stable to changing conditions, thus enabling robust augmented reality and autonomous navigation for robots. Given the strong overlap of interests in these areas, we hope that this paper helps to bring research on visual localization and place recognition in computer vision and robotics closer together. We will extend the benchmark over time with new datasets and new challenges.

## 2. Related Work

**2D Image-based Localization.** Purely 2D image-based techniques are still predominantly used in both computer vision and robotics in the context of place recognition [2, 16, 59, 72, 77] and loop-closure detection [18, 22, 50]. While not directly providing a pose estimate, an approximation can be obtained from the pose of the database photo considered to be most similar to the query. 2D image-based techniques are

especially relevant in the context of this paper due progress on robustness in changing conditions [2, 16, 51, 72, 77].

2D image-based localization methods typically employ standard retrieval techniques such as Bag-of-Words (BoW) representations with inverted files [14, 68], which are still effective at city-scale [5, 59, 78]. As in the standard image retrieval pipeline, relevant images are shortlisted and geometrically verified [5, 14, 54, 59, 75, 78]. Compact representations, *e.g.*, VLAD or Fischer Vectors [4, 29, 31, 76] or recent CNN-based trainable descriptors [2, 57], are preferred when a database covers a large area.

FAB-MAP [18] follows an image retrieval approach based on the BoW paradigm and has explicitly been designed for loop-closure detection. The method explicitly models the co-occurrence probability of different visual words in order to improve retrieval performance. FAB-MAP is the de-facto baseline approach for loop-closure detection in robotics [20, 36], where robust place recognition in changing conditions is critical for long-term navigation of autonomous vehicles [16, 37, 46, 51, 72, 77]. A recent survey of place recognition approaches is presented in [40].

**3D Structure-based Localization.** 3D structure-based methods [34, 35, 58, 60, 61, 73, 84] employ a 3D scene model computed via SfM, where each 3D point is associated with a local image descriptor. The 2D-3D correspondences required for camera pose estimation via an  $n$ -point-pose solver, *e.g.*, the 3-point-pose solver for calibrated cameras [21, 32], can then be obtained via descriptor matching.

**Learning-based Localization.** Recently, a number of end-to-end learning approaches have been proposed to solve both loop-closure detection [16, 45, 70, 72] and pose estimation [17, 30, 80] in large-scale environments across long time periods. Such methods learn classifiers/regressors, *e.g.*, based on a BoW representation [12, 26] or using CNNs [30, 81] to distinguish between images belonging to different places [81] or to directly regress 2D-3D matches [10, 66] or camera poses [17, 30, 80].

Other approaches use learning to improve components of conventional approaches. Chen *et al.* model place recognition as a classification task to learn descriptors that are stable in appearance over time [16], and related methods learn features or image regions that are geometrically stable [49, 51]. Linegar *et al.* train SVM classifiers for each place to identify mid-level features that can be used for feature matching between seasons [37].

**Benchmark Datasets.** 6DOF localization approaches typically evaluate on photo-community collections, *e.g.*, images from Flickr, such as the Dubrovnik and Rome [35] or Landmarks [34] datasets. In contrast to such datasets, which often also contain some night-time images [56], our night-time queries are distributed over our models. This results in a harder night-day matching problem as queries do not

focus on a few selected, well-photographed landmarks.

Methods for truly large-scale localization are evaluated on the 3D models of San Francisco from [34]. Learning-based methods are usually validated on the indoor 7Scenes [66] or the outdoor Cambridge Landmarks [30] dataset. While both provide ground truth poses, neither covers changing environmental conditions.

Compared to other datasets used for day-night place recognition such as Tokyo 24/7 [77] and the AMOS web-cam dataset [27], we provide 6DOF ground truth pose for each night-time query image. In addition, for each night-time query we provide a day-time query image taken from a similar pose as a reference.

For autonomous driving applications a number of datasets are available [8, 53], including datasets that focus on long-term appearance change [6, 71], but few offer a benchmarking service for comparison of results. The well-known KITTI dataset [23] offers benchmarking for components of visual navigation including stereo, optical flow, and visual odometry, but does not provide 3D ground truth nor challenging appearance changes over time.

### 3. Benchmark Datasets for 6DOF Localization

This section focusses on the main contribution of the paper, the creation of two new datasets that are used to explicitly benchmark the impact of different viewing conditions on the localization rate, *i.e.*, the number of localized images, and pose estimation accuracy. We detail the challenges posed by each dataset and why it is important to overcome these challenges to enable stable and robust image-based localization “in the wild”. For each dataset, we explain how we generated reference poses for each query image.

#### 3.1. The Aachen Day-Night Dataset

Our *Aachen Day-Night* dataset significantly extends upon the Aachen localization dataset from [62] by adding additional images, especially night-time query images, and constructing ground truth poses for the queries. Tab. 1 provides details on the different versions of the dataset.

The original, publicly available, Aachen dataset consists of 4,479 database images and 369 query images, 10 of which were captured at night, taken in the old inner city of Aachen, Germany. The database images were captured with multiple compact and DSLR cameras and the query images were taken with a Motorola Milestone mobile phone. A 3D model containing 3,047 database images and 1.54M 3D points was reconstructed with Bundler [69]. No ground truth camera poses for the queries are provided.

To obtain a single connected reconstruction that contains all database images, we recorded multiple video sequences from which we extracted frames. In addition, we took another 475 day-time query images with a Google Nexus 4 and a Google Nexus 5X smart phone, and 103 night-time



Figure 2. Example query images for the *Aachen Day-Night* dataset (top) and the *RobotCar Seasons* dataset (bottom).

query photos with the Nexus 5X. In contrast to the night-time pictures taken by the Milestone, which are extremely dark and noisy due to the camera’s poor quality, we took these new photos using Android’s software HDR functionality. As a result, these new night-time queries are well-lit, providing a chance to re-detect the same features as detected in the day-time images, as shown in the top row of Fig. 2.

We used COLMAP [63] to create a 3D reconstruction containing 4,328 database images, 824 day-time query photos, and 2,369 video frames as well as 2.43M 3D points and 17.56M feature observations. Query images taken with the same camera share their intrinsic calibration and thus reconstructed images provide the calibration for the night-time queries as well. This base model was then registered against the original Aachen model by fitting a similarity transformation through the database image positions, enabling us to recover the model’s scale in meters.

The poses of the day-time queries registered in the base model serve as ground truth. We obtained a 3D database model that can be used for querying by removing all video frames and the query images. 3D points visible in only a single remaining camera were removed as well to avoid any trace of the query images in the model [35]. The resulting 3D model, shown in Fig. 3, has 4,328 database images, 1.65M 3D points, and 10.55M feature observations.

**Ground Truth for Night-time Queries.** While the base model also contained 83 night-time images, their poses estimates were rather inaccurate. Consequently, we decided to obtain reference poses through manual annotation.

For each of the 103 night-time photos taken by the Nexus 5X, we manually selected an equivalent day-time image from the base model taken from a similar viewpoint. From the base model, we obtained the 3D points visible in these day-time photos and projected the points into these images. We then manually selected 10 to 30 pixel positions in each night-time query that correspond to the projections of the points. Using the resulting 2D-3D matches, the cam-

	# model images	# 3D points	# observations	# day-time queries	# night-time queries	query image resolutions
Aachen [62]	3,047	1.54M	7.28M	359 (0)	10 (0)	$1024 \times 768$
Aachen Day-Night Base	7,604	2.43M	17.56M	834 (824)	113 (98)	$1024 \times 768, 1600 \times 1200$
Aachen Day-Night	4,328	1.65M	10.55M	824 (824)	98 (98)	$1024 \times 768, 1600 \times 1200$

Table 1. Detailed statistics for the *Aachen Day-Night* dataset on the number of images in the 3D model, 3D points, feature observations, day-time queries, and night-time query images. The number of queries with ground truth poses is indicated by the number in parentheses.



Figure 3. The 3D model of the *Aachen Day-Night* dataset, covering an area of  $82,859 \text{ m}^2$ . Database image, day-time query, and night-time query are shown in red, green, and blue, respectively.

era poses of the night-time photos were computed using a 3-point-pose solver [21, 32] inside a RANSAC loop [21], followed by non-linear optimization of the re-projection errors. We visually verified the quality of each camera pose by projecting all the 3D points visible from the equivalent day-time image to the night-time query. Finally, we selected 98 of the 103 night-time images captured with the Nexus 5X as queries with good pose estimates.

**Covered Scenarios.** The *Aachen Day-Night* dataset covers a night-to-day matching scenario, where the database was built solely from day-time imagery. All images were taken in an area inaccessible to cars and typically crowded with pedestrians. Thus, obtaining the database images is significant work and one would like to avoid having to capture database photos at both day and night. As such, the *Aachen Day-Night* dataset poses a realistic challenge.

All images in the dataset were taken with hand-held cameras. The dataset thus represents a scenario where a user would like to gain information about what an image depicts, *e.g.*, in the context of an AR application or to automatically annotate holiday photos [34].

### 3.2. The RobotCar Seasons Dataset

Our *RobotCar Seasons* dataset is based on a subset of the publicly available Oxford RobotCar Dataset [43], which consists of over 20M images recorded from an autonomous vehicle platform over a 12 month period in Oxford, UK. Out of the 100 available traversals of the 10km route, we select one reference traversal (in overcast conditions) and nine query traversals, shown in Tab. 2. The query traversals

condition	recorded	images		
		individual	positions	sequences
overcast (reference)	28 Nov 2014	20,862	8,707	-
dawn	16 Dec 2014	1,449	483	54
dusk	20 Feb 2015	1,182	394	48
night	10 Dec 2014	1,314	438	49
night+rain	17 Dec 2014	1,320	440	51
overcast (summer)	22 May 2015	1,389	463	52
overcast (winter)	13 Nov 2015	1,170	390	49
rain	25 Nov 2014	1,263	421	50
snow	3 Feb 2015	1,467	489	56
sun	10 Mar 2015	1,380	460	51
total query	-	11,934	3,978	460

Table 2. Detailed statistics for the *RobotCar Seasons* dataset. We used images from the *overcast (reference)* traversal to build a 3D scene model. For each of the query sequences, we report the total number of query images taken by all three individual cameras, the number of positions at which images were taken, and the number of temporally continuous query sequences.

were chosen to cover a wide range of illumination conditions, including direct sun, night, rain and snow, as well as long-term seasonal changes from winter to summer. For both the reference and query images we used the three synchronised Point Grey Grasshopper2 cameras mounted to the left, rear, and right of the RobotCar, each providing synchronized  $1024 \times 1024$  pixel images covering a  $105^\circ$  field-of-view (FoV). Both the intrinsic calibrations of the cameras and their relative extrinsic calibrations are known.

The reference traversal contains 26,121 images taken at 8,707 positions, with 1m between successive positions. Building a consistent 3D model from this data is very challenging: there is no visual overlap between the three cameras, resulting in only few visual constraints between them, and the sheer number of images makes constructing a single consistent 3D model computationally challenging.

Rather than constructing a single consistent 3D model, we built 49 non-overlapping local submaps (each covering a 100m trajectory) to use as reference databases for localization. For each submap, we initialized the database camera poses using vehicle positions reported by the inertial navigation system (INS) mounted on the RobotCar. We then iteratively triangulated 3D points from feature matches, merged tracks, and refined both structure and poses using bundle adjustment. The reconstructions were then registered against the INS poses, thus preserving metric scale. The resulting model, shown in Fig. 4, contains a total of 20,862 reference images and a combined total of 6.77M 3D points triangulated from 36.15M observations.

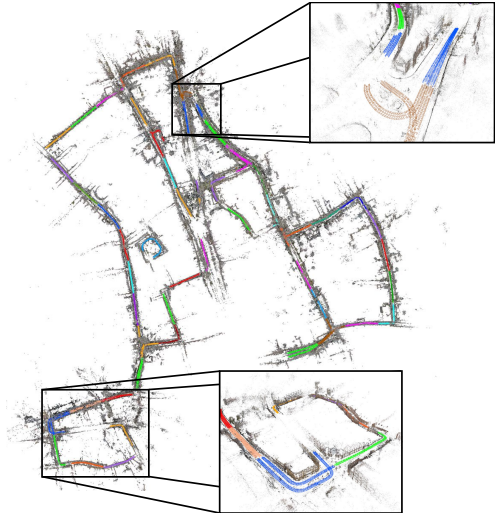


Figure 4. The 3D model of the *RobotCar Seasons* dataset, a 10km route through central Oxford, UK. Different colors encode the 49 individual submaps.

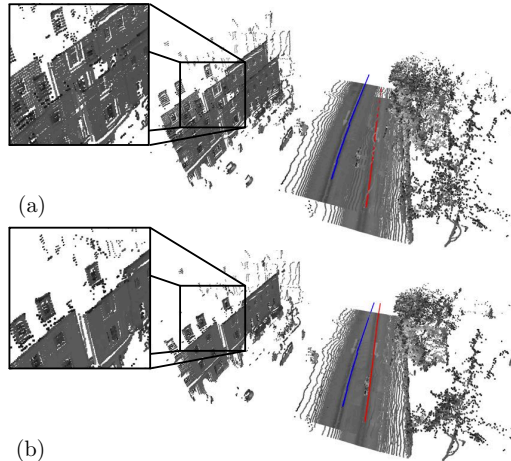


Figure 5. Ground truth alignment for the *RobotCar Seasons* dataset. The 3D LIDAR point cloud (grey) is shown (a) before and (b) after alignment of the two INS trajectories (red and blue).

In order to obtain query images, we selected reference positions inside the 49 submaps and gathered all images from the nine query traversals whose INS poses fall within 10m of one of the positions. This resulted in 11,934 images in total, where triplets of images were captured at 3,978 locations. In addition to considering individual images and triplets of photos taken by the three cameras, we also grouped the queries into 460 temporal sequences based on the timestamps of the images.

**Ground Truth Poses for the Queries.** Due to the problems of obtaining strong constraints between day-time and night-time images, we decided to not use SfM to compute ground truth poses for the queries. We used the LIDAR scanners mounted to the vehicle to build local 3D point clouds for each of the 49 locations, which were matched

to a 3D point cloud built at each reference location using iterative closest point (ICP) [7] to eliminate the offset caused by GPS drift, shown in Fig. 5. Many of the ICP matches needed to be manually adjusted and verified to account for changes in scene structure over time (often due to building construction and road layout changes). The final median RMS errors between matched LIDAR point clouds was under 10cm in translation and 0.5° in rotation across all locations. Ground truth poses for the 11,934 query images were then derived using the corrected INS trajectory and the known extrinsics of the cameras on the vehicle.

**Covered Scenarios.** Reliable operation independent of weather or seasonal effects is a key requirement for self-driving cars. The *RobotCar Seasons* dataset focusses on localization performance and loop-closure detection, *e.g.*, in the context of SLAM, for autonomous vehicles in this scenario. Compared to the *Aachen Day-Night* dataset, the query images of the *RobotCar Seasons* dataset exhibit less variability in viewpoints (as the car is restricted to driving on the roads) but a larger variance in viewing conditions. Also, it allows us evaluate the benefits of multiple images captured simultaneously, as well as sequences of images, in comparison to querying with individual photos.

## 4. Reference Algorithms

In this section, we describe the state-of-the-art algorithms that we use for experimental evaluation. We group the different methods based on common characteristics. The code for all methods used for evaluation is publicly available.

### 4.1. 2D Image-based Localization

We use three 2D image-based methods for experimental evaluation, namely DenseVLAD [77], NetVLAD [2], and FAB-MAP [18]. DenseVLAD aggregates (RootSIFT) descriptors [3] densely extracted from an image into a compact Vector of Locally Aggregated descriptors (VLAD) [28]. As shown in [77], this strategy leads to an image representation that is more robust to day-night variations than methods based on sparse features.

The NetVLAD representation is a differentiable variant of the VLAD method, enabling convolutional neural networks (CNN) to learn compact image representations. NetVLAD learns to pool CNN features into a single descriptor and the models provided by [2] were trained from Google Street View Time Machine images, *i.e.*, photos depicting places over a long period of time.

For FAB-MAP we use the open source implementation [24], which allows us to train a visual vocabulary and Chow-Liu tree specifically for each dataset.

## 4.2. 3D Structure-based Localization

We evaluate Active Search [60, 61], a structure-based approach that utilizes prioritized matching to accelerate the localization process. Active Search has been shown to work well, both in terms of run-time efficiency and the number of localized images, on datasets comparable in size to the *Aachen Day-Night* and *RobotCar Seasons* models [61].

In addition, we evaluate a structure-based localization strategy based on local SfM reconstructions [65]. Given a reference image from the database, *e.g.*, from image retrieval, we determine a small set of database images similar to the reference. After exhaustive pairwise image matching, we attempt to build a local 3D model using either COLMAP or VisualSfM [83]. The resulting reconstruction is then registered against the database 3D model, using the known poses of the database images to estimate a similarity transformation. This registration process provides an estimate of the query camera pose in case that the local reconstruction contains the query image. Compared with Active Search, which globally matches the features found in the query photo against all 3D model points, this strategy only needs to solve local matching problems. We evaluate two variants: The first uses upright RootSIFT features (LocalSfM) while the other (DenseSfM) uses the same CNN features as NetVLAD, extracted on a regular grid<sup>1</sup>. For each night-time query, we use the 20 database images who share the largest number of 3D points with the equivalent day-time image.

## 4.3. Trajectory-based Localization

**3D Structure-based Trajectory.** At each time step, the RobotCar dataset provides an image triplet, taken with two side- and a back-facing camera. Rather than estimating a pose for each image individually, we can model the multi-camera system as a generalized camera [55], *i.e.*, a camera with multiple centers of projection. The poses of a triplet are estimated simultaneously, preserving the known extrinsic calibration between cameras, using a generalized absolute camera pose solver [33]. This strategy uses the matches found by Active Search for each individual query.

Simultaneously, the movement of a camera, or a multi-camera system, also defines a generalized camera [11]. Assuming the relative poses between subsequent time-steps are known, *e.g.*, from SLAM [11], we also evaluate utilizing all image triplets in a sequence for pose estimation.

Treating multiple cameras as a generalized camera offers the possibility of accumulating matches over multiple images. Consequently, we would expect these approaches to work better under strong appearance changes, where fewer

<sup>1</sup>We view these methods as extensions of the approaches used in NetVLAD and DenseVLAD to SfM. See the appendix for more detailed descriptions of the LocalSfM and DenseSfM methods.

matches are found for each individual image.

**2D Image-based Trajectory.** Trajectory-based approaches have also been applied to solve the loop-closure problem for robotics applications in [42, 46, 52]. Requiring a matched sequence of images in the correct order significantly reduces false positive rates in comparison to single-image retrieval approaches, producing impressive results including direct day-night matches [46]. To test trajectory-based loop-closure approaches we evaluate the OpenSeqSLAM implementation [71].

## 4.4. Learning-based Localization

We attempted to evaluate the recent PoseNet [30] approach on both datasets. We split the database images from each dataset into a 75%-25% split of training and validation images, and experimented with a range of  $\beta$  values between 500 and 2000. However, after more than 500 epochs the lowest median pose errors on the *validation* sets still exceeded 35m and 60° for both datasets.

We speculate that the network architecture provided in the reference PoseNet implementation does not scale well to datasets of this size; note that Walch *et al.* have shown that learning-based methods [17, 30, 80] have yet to outperform Active Search on a set of standard benchmarks [80].

## 5. Experimental Evaluation

This section presents the second major contribution of this paper, a detailed experimental evaluation on the effect of changing conditions on the performance of visual localization techniques. We first define the metrics used in our experiments before evaluating the reference algorithms described in Sec. 4 on our two novel datasets.

**Evaluation Measures.** We measure the performance of visual localization and place recognition algorithms using two metrics, **localization rate** and **pose accuracy**.

The **localization rate** measures how many of the query images can be localized. For the structure-based approaches, an image is considered successfully localized if its camera pose, estimated via RANSAC [21], has at least 12 inliers [34, 35, 60, 61] or if a query image is contained in a local SfM model. We report both the absolute number as well as the percentage of localized images.

We measure the **pose accuracy** of the different methods by determining the error in estimated camera position and orientation compared to the ground truth pose. For the **position error**, this quantity is measured as the Euclidean distance  $\|c_{\text{est}} - c_{\text{gt}}\|_2$  between the estimated  $c_{\text{est}}$  and ground truth position  $c_{\text{gt}}$ . The **orientation error** is computed from the estimated and ground truth camera rotation matrices  $R_{\text{est}}$  and  $R_{\text{gt}}$ . We determine the orientation error as the minimal rotation angle  $\alpha$  required to align both rotations. Here,  $\alpha$  is

defined as the rotation angle of the axis-angle representation of the relative rotation  $R_{\text{est}}^{-1}R_{\text{gt}}$ .

## 5.1. Evaluation on the Aachen Day-Night dataset

**Day-time Queries.** We evaluate Active Search, NetVLAD, DenseVLAD, and FAB-MAP on the 824 day-time queries of the Aachen Day-Night dataset<sup>2</sup>. Fig. 6(a-b) show the cumulative distribution of the position and orientation errors. Unsurprisingly, Active Search performs significantly better than the 2D image-based since the latter only approximate the camera pose of the query. Interestingly, FAB-MAP performs significantly worse than the two VLAD-based methods. Aggregating images features into a single descriptor is less robust to viewpoint changes, forcing DenseVLAD and NetVLAD to select database images taken closer to the query, resulting in a better pose accuracy. Active Search localizes 798 (96.84%) of the queries with median position and orientation errors of 19cm and 0.25°, respectively, establishing it as a strong baseline.

**Night-time Queries.** In the next experiment, we evaluate localization performance on the 98 night-time query images. The localization rate of Active Search drops significantly to only 47 (47.96%) images. As shown in Fig. 6(c-d), Active Search is either able to localize an image rather accurately (median errors of 66cm and 1.49°) or not at all. Since both NetVLAD and DenseVLAD do not rely on local feature matches, they are able to localize more images, albeit at the cost of a higher pose error. FAB-MAP fails to localize images at night since the visual vocabulary was trained on day-time images only.

In addition to Active Search, DenseVLAD, NetVLAD, and FAB-MAP, we evaluate the two approaches based on local SfM reconstruction (*c.f.* Sec. 4.2). As can be seen, using a local reconstruction with the upright RootSIFT features (LocalSfM) boosts the localization rate compared to Active Search. This shows that Active Search loses matches between dissimilar descriptors due to solving a harder global matching problem. DenseSfM provides even better localisation performance at the cost of higher pose error. Dense feature extraction foregoes feature detection, enabling DenseSfM to establish correspondences even if the detector does not provide repeatable detections. The price is a worse pose quality resulting from the fact that the CNN features used by NetVLAD are less accurately localized in the images, leading to less accurate SfM reconstructions.

## 5.2. Evaluation on the RobotCar Seasons dataset

**Structure-based Localization.** In an initial experiment, we evaluated the localization rates obtained when querying

<sup>2</sup>Notice that trajectory-based methods are not applicable on the Aachen dataset as all queries are individual photos.

with each image independently. We observed that significantly better rates are obtained when using the rear camera compared to the two side-facing cameras (*c.f.* supp. material). In the following we only use images taken by the rear camera for single image queries. As shown in Tab. 3, Active Search performs well over most of the conditions, the exceptions being *dawn* and *sun* (where the cameras are often in direct sunlight) and the two night conditions. Since the RobotCar cameras do not provide HDR images, the performance is worse for night-time queries compared to Aachen.

Tab. 3 also shows results for using a generalized camera, formed by the image triplet taken at a single time step, for pose estimation. Combining feature matches from multiple images significantly boosts localization rates under challenging conditions, but has little impact otherwise (both on the easier conditions and on pose accuracy). Thus, using a multi-camera system is recommended for robust localization under changing conditions. For both single and generalized camera queries, we observe that night-time images can either be localized rather accurately or not at all.

As a further experiment, we analyze localization of short sequences consisting of image triplets taken at successive timestamps. Tab. 4 shows the results when using individual images as queries (*single*); a generalized camera formed by image triplets from the same timestamp (*generalized*); and all triplets in the sequence (*sequence*). Using the full sequence significantly improves the localization rates for difficult sequences but with only a small increase in pose accuracy (*c.f.* supp. material).

**Comparison of Image- and Structure-based Methods.** As a final experiment, we compare structure-based methods using single query images (*ActiveSearch*) and image triplets per timestamp (*ActiveSearch+GC*) with 2D image-based methods. As for Tab. 4, we aggregate the night-time and day-time traversals, but report results on an image- rather than sequence-level. The results of the comparison are shown in the bottom row of Fig. 6. As can be seen, DenseVLAD clearly outperforms both FAB-MAP and SeqSLAM. For day-time queries, Active Search (with generalized cameras) performs best. Interestingly, DenseVLAD achieves the best localization rates and pose quality on the night-time sequences. DenseVLAD thereby benefits from the fact that the car travels along fixed roads, leading to little change in camera viewpoint. As such, the pose of the most similar database image provides a very good approximation to the pose of the query.

SeqSLAM performed poorly on day-time images from the RobotCar due to the large amount of perceptual aliasing between locations with similar appearances, *e.g.*, straight roads with identical building facades, which are common in Oxford and difficult to distinguish using low resolution images. The co-occurrence model used by FAB-MAP yields better performance in the presence of spatial aliasing dur-

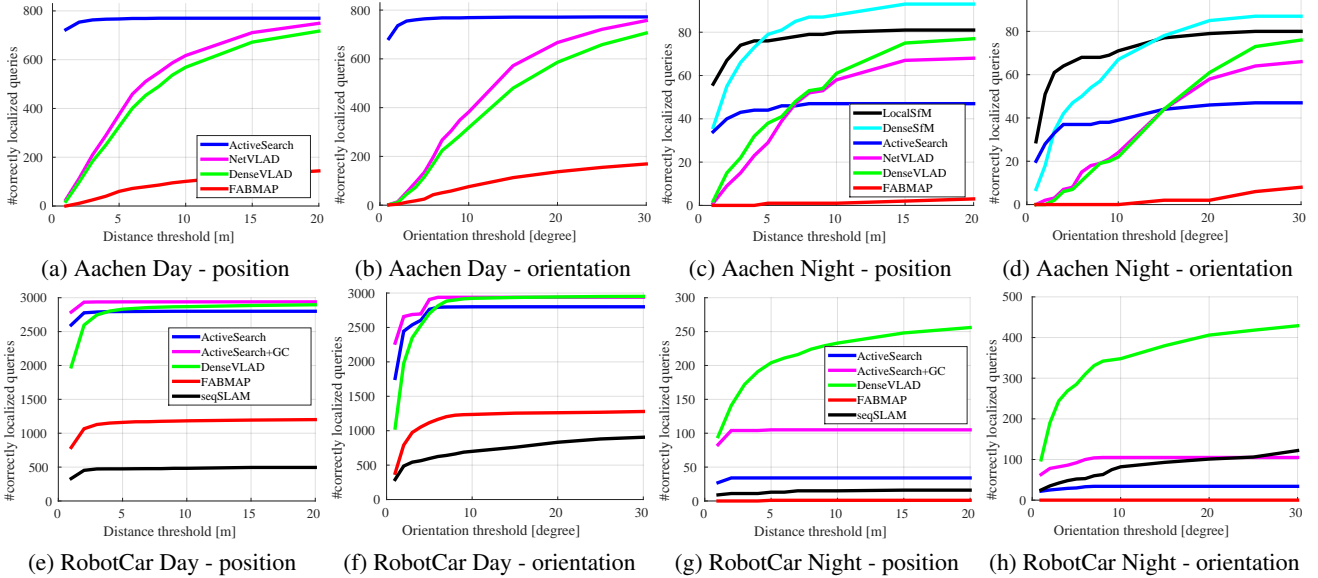


Figure 6. Evaluation on the **Aachen Day-Night** (top row) and **RobotCar Seasons** (bottom row) datasets: (a/c/e/g) and (b/d/f/h) show the number of day- / night-time query images whose position, respectively orientation, estimate is within a threshold of the ground truth.

condition	loc. rate	single image queries				generalized camera queries				
		Quantiles errors: position [m], orientation [°]	25%	50%	75%	95%	Quantiles errors: position [m], orientation [°]	25%	50%	75%
dawn	432 (89.44%)	0.18, 0.40	0.31, 0.61	0.50, 0.93	1.16, 4.75	<b>460 (95.24%)</b>	0.16, 0.36	0.24, 0.50	0.40, 0.73	1.08, 4.74
dusk	378 (95.94%)	0.18, 0.64	0.26, 0.78	0.41, 0.96	1.02, 4.25	378 (95.94%)	0.15, 0.59	0.22, 0.71	0.34, 0.84	1.02, 4.36
night	15 (3.42%)	0.49, 0.74	0.61, 0.94	0.81, 3.36	0.96, 6.05	<b>38 (8.68%)</b>	0.38, 0.64	0.64, 0.86	0.88, 2.57	1.45, 6.17
night+rain	19 (4.32%)	0.26, 0.58	0.33, 0.69	0.41, 1.08	1.42, 1.56	<b>67 (15.23%)</b>	0.26, 0.40	0.40, 0.62	0.63, 1.71	1.32, 5.35
overcast (summer)	442 (95.46%)	0.24, 0.84	0.36, 1.06	0.59, 1.45	1.09, 4.14	<b>455 (98.27%)</b>	0.20, 0.75	0.32, 0.89	0.48, 1.09	0.95, 4.23
overcast (winter)	365 (93.59%)	0.21, 0.68	0.32, 0.89	0.45, 1.20	1.25, 4.10	368 (94.36%)	0.18, 0.73	0.27, 0.88	0.40, 1.11	0.96, 4.28
rain	409 (97.15%)	0.15, 0.73	0.24, 0.90	0.42, 1.11	0.94, 4.96	410 (97.39%)	0.15, 0.50	0.23, 0.67	0.36, 0.88	0.91, 5.01
snow	455 (93.05%)	0.18, 0.57	0.29, 0.78	0.44, 1.16	1.14, 4.20	<b>466 (95.30%)</b>	0.14, 0.53	0.22, 0.70	0.36, 0.91	1.04, 4.30
sun	314 (68.26%)	0.20, 0.74	0.33, 1.01	0.57, 1.45	1.30, 4.15	<b>402 (87.39%)</b>	0.16, 0.68	0.27, 0.83	0.46, 1.06	1.03, 4.24

Table 3. **Active Search on the RobotCar Seasons dataset:** We report the localization rate as the number and percentage of localized queries as well as the quantiles on the pose errors. Using *generalized cameras* formed by image triplets improves localization rates.

condition	# sequences	localization rate		
		single	generalized	full sequence
all day	360	334 (92.8%)	342 (95%)	346 (96.1%)
all night	100	9 (9%)	24 (24%)	41 (41%)

Table 4. Using Active Search to localize **sequences** on the **RobotCar Seasons** dataset. We report results for using a single camera per timestamp (*single*), image triplets per timestamp (*generalized*), and using all triplets in the sequence (*full sequence*).

ing the day, but the visual bag-of-words approach is limited when matching between day and night. SeqSLAM’s whole-image sequence matches performed better than FAB-MAP when matching night-time query sequences to day-time reference images, but did not match the performance of DenseVLAD.

## 6. Conclusion & Lessons Learned

In this paper we have introduced two challenging new benchmark datasets for visual localization. The novel datasets allow us, for the first time, to analyze the impact of changing conditions on the accuracy of 6DOF camera

pose estimation. The extensive experiments performed in this paper allow us to draw interesting conclusions: (i) classical feature-based methods such as Active Search are very robust to most viewing conditions and can provide highly accurate pose estimates, hence are readily applicable to autonomous driving scenarios. (ii) localizing night-time images against a database built from day-time photos is a very challenging problem, more so than varying weather conditions. Interestingly, there does not seem to be a gradual decrease in pose quality for feature-based methods as they either localize an image accurately or not at all. (iii) dense feature extraction is the best strategy for localizing more night-time images. Finding ways to handle dense feature matching efficiently (and potentially at scale) is thus an interesting avenue for future research. (iv) if multiple images, *e.g.*, a multi-camera system or an image sequence, are available, using them for pose estimation significantly boosts the localization rates but not necessarily pose accuracy.

We plan to extend our benchmark with scenes not yet covered in our datasets such as natural scenes outside of urban environments (for agricultural robotics) and indoor

scenes (for AR-based navigation). We will eventually make our datasets publicly available to encourage work on visual localization under changing conditions.

**Acknowledgements.** This work was partially supported by ERC grant LEAP (no. 336845), CIFAR Learning in Machines & Brains program, ESIF, OP Research, development and education Project IMPACT No. CZ.02.1.01/0.0/0.0/15\_003/0000468, JSPS KAKENHI Grant Number 15H05313, and EPSRC Programme Grant EP/M019918/1.

## References

- [1] S. Agarwal, K. Mierle, and Others. Ceres solver. <http://ceres-solver.org>. 13
- [2] R. Arandjelović, P. Gronat, A. Torii, T. Pajdla, and J. Sivic. NetVLAD: CNN architecture for weakly supervised place recognition. In *Proc. CVPR*, 2016. 2, 5, 11
- [3] R. Arandjelović and A. Zisserman. Three things everyone should know to improve object retrieval. In *Proc. CVPR*, 2012. 5, 11, 12, 13
- [4] R. Arandjelović and A. Zisserman. All about VLAD. In *Proc. CVPR*, 2013. 2
- [5] R. Arandjelović and A. Zisserman. DisLocation: Scalable descriptor distinctiveness for location recognition. In *Proc. ACCV*, 2014. 2
- [6] H. Badino, D. Huber, Y. Park, and T. Kanade. Real-Time Topometric Localization. In *Proc. ICRA*, 2012. 3
- [7] P. J. Besl and N. D. McKay. Method for registration of 3-D shapes. In *Robotics-DL tentative*, pages 586–606. International Society for Optics and Photonics, 1992. 5
- [8] J.-L. Blanco-Claraco, F.-Á. Moreno-Dueñas, and J. González-Jiménez. The Málaga urban dataset: High-rate stereo and LiDAR in a realistic urban scenario. *Intl. J. of Robotics Research*, 33(2):207–214, 2014. 3
- [9] A. Bosch, A. Zisserman, and X. Munoz. Image classification using random forests and ferns. In *Proc. ICCV*, 2007. 12
- [10] E. Brachmann, F. Michel, A. Krull, M. Y. Yang, S. Gumhold, and C. Rother. Uncertainty-driven 6d pose estimation of objects and scenes from a single rgb image. In *Proc. CVPR*, 2016. 2
- [11] F. Camposeco, T. Sattler, and M. Pollefeys. Minimal Solvers for Generalized Pose and Scale Estimation from Two Rays and One Point. In *Proc. ECCV*, 2016. 6
- [12] S. Cao and N. Snavely. Graph-based discriminative learning for location recognition. In *Proc. CVPR*, 2013. 2
- [13] S. Cao and N. Snavely. Minimal Scene Descriptions from Structure from Motion Models. In *Proc. CVPR*, 2014. 1
- [14] D. Chen, S. Tsai, V. Chandrasekhar, G. Takacs, H. Chen, R. Vedantham, R. Grzeszczuk, and B. Girod. Residual enhanced visual vectors for on-device image matching. In *Asilomar*, 2011. 2
- [15] D. M. Chen, G. Baatz, K. Koeser, S. S. Tsai, R. Vedantham, T. Pylvanainen, K. Roimela, X. Chen, J. Bach, M. Pollefeys, B. Girod, and R. Grzeszczuk. City-scale landmark identification on mobile devices. In *Proc. CVPR*, 2011. 11
- [16] Z. Chen, A. Jacobson, N. Sünderhauf, B. Upcroft, L. Liu, C. Shen, I. D. Reid, and M. Milford. Deep learning features at scale for visual place recognition. *ICRA*, 2017. 1, 2
- [17] R. Clark, S. Wang, A. Markham, N. Trigoni, and H. Wen. VidLoc: 6-DoF Video-Clip Relocalization. *arXiv:1702.06521*, 2017. 2, 6
- [18] M. Cummins and P. Newman. FAB-MAP: Probabilistic Localization and Mapping in the Space of Appearance. *Intl. J. of Robotics Research*, 27(6):647–665, 2008. 2, 5, 11
- [19] M. Cummins and P. Newman. Appearance-only slam at large scale with fab-map 2.0. *The International Journal of Robotics Research*, 30(9):1100–1123, 2011. 11
- [20] J. Engel, T. Schöps, and D. Cremers. LSD-SLAM: Large-scale direct monocular SLAM. In *Proc. ECCV*, 2014. 2
- [21] M. Fischler and R. Bolles. Random Sampling Consensus: A Paradigm for Model Fitting with Application to Image Analysis and Automated Cartography. *Commun. ACM*, 24:381–395, 1981. 2, 4, 6, 12
- [22] D. Gálvez-López and J. D. Tardos. Bags of binary words for fast place recognition in image sequences. *IEEE Transactions on Robotics*, 28(5):1188–1197, 2012. 2
- [23] A. Geiger, P. Lenz, C. Stiller, and R. Urtasun. Vision meets robotics: The KITTI dataset. *Intl. J. of Robotics Research*, 32(11):1231–1237, 2013. 3
- [24] A. Glover, W. Maddern, M. Warren, S. Reid, M. Milford, and G. Wyeth. openFABMAP: An open source toolbox for appearance-based loop closure detection. In *Proc. ICRA*, 2012. 5, 11
- [25] Google. Google Tango. [get.google.com/tango](http://get.google.com/tango). 1
- [26] P. Gronat, J. Sivic, G. Obozinski, and T. Pajdla. Learning and calibrating per-location classifiers for visual place recognition. *IJCV*, 118(3):319–336, 2016. 2
- [27] N. Jacobs, N. Roman, and R. Pless. Consistent Temporal Variations in Many Outdoor Scenes. In *Proc. CVPR*, 2007. 3
- [28] H. Jégou, M. Douze, C. Schmid, and P. Pérez. Aggregating local descriptors into a compact image representation. In *Proc. CVPR*, 2010. 5
- [29] H. Jégou, F. Perronnin, M. Douze, J. Sánchez, P. Pérez, and C. Schmid. Aggregating local image descriptors into compact codes. *IEEE PAMI*, 34(9):1704–1716, Sep 2012. 2
- [30] A. Kendall, M. Grimes, and R. Cipolla. PoseNet: A Convolutional Network for Real-Time 6-DOF Camera Relocalization. In *Proc. ICCV*, 2015. 2, 3, 6
- [31] H. J. Kim, E. Dunn, and J. Frahm. Predicting good features for image geo-localization using per-bundle VLAD. In *Proc. ICCV*, pages 1170–1178, 2015. 2
- [32] L. Kneip, D. Scaramuzza, and R. Siegwart. A Novel Parametrization of the Perspective-Three-Point Problem for a Direct Computation of Absolute Camera Position and Orientation. In *Proc. CVPR*, 2011. 2, 4
- [33] G. H. Lee, B. Li, M. Pollefeys, and F. Fraundorfer. Minimal solutions for the multi-camera pose estimation problem. *Intl. J. of Robotics Research*, 34(7):837–848, 2015. 6, 12
- [34] Y. Li, N. Snavely, D. Huttenlocher, and P. Fua. Worldwide Pose Estimation Using 3D Point Clouds. In *Proc. ECCV*, 2012. 1, 2, 3, 4, 6

[35] Y. Li, N. Snavely, and D. P. Huttenlocher. Location Recognition using Prioritized Feature Matching. In *Proc. ECCV*, 2010. 1, 2, 3, 6

[36] C. Linegar, W. Churchill, and P. Newman. Work smart, not hard: Recalling relevant experiences for vast-scale but time-constrained localisation. In *Proc. ICRA*, 2015. 2

[37] C. Linegar, W. Churchill, and P. Newman. Made to measure: Bespoke landmarks for 24-hour, all-weather localisation with a camera. In *Proc. ICRA*, 2016. 2

[38] C. Liu, J. Yuen, A. Torralba, J. Sivic, and W. T. Freeman. SIFT Flow: Dense correspondence across different scenes. In *Proc. ECCV*, pages 28–42, 2008. 12

[39] D. Lowe. Distinctive Image Features from Scale-Invariant Keypoints. *IJCV*, 60(2), 2004. 11, 12, 13

[40] S. Lowry, N. Sünderhauf, P. Newman, J. J. Leonard, D. Cox, P. Corke, and M. J. Milford. Visual place recognition: A survey. *IEEE Transactions on Robotics*, 32(1):1–19, 2016. 1, 2

[41] S. Lynen, T. Sattler, M. Bosse, J. Hesch, M. Pollefeys, and R. Siegwart. Get Out of My Lab: Large-scale, Real-Time Visual-Inertial Localization. In *RSS*, 2015. 1

[42] W. Maddern, M. Milford, and G. Wyeth. CAT-SLAM: probabilistic localisation and mapping using a continuous appearance-based trajectory. *Intl. J. of Robotics Research*, 31(4):429–451, 2012. 6

[43] W. Maddern, G. Pascoe, C. Linegar, and P. Newman. 1 Year, 1000km: The Oxford RobotCar Dataset. *Intl. J. of Robotics Research*, 36(1):3–15, 2017. 4

[44] Microsoft. Microsoft HoloLens. [www.microsoft.com/microsoft-hololens](http://www.microsoft.com/microsoft-hololens). 1

[45] M. Milford, S. Lowry, N. Sünderhauf, S. Shirazi, E. Pepperell, B. Upcroft, C. Shen, G. Lin, F. Liu, C. Cadena, et al. Sequence searching with deep-learnt depth for condition-and viewpoint-invariant route-based place recognition. In *Workshop on Computer Vision in Vehicle Technology (CVVT)*, *CVPR*, 2015. 2

[46] M. J. Milford and G. F. Wyeth. SeqSLAM: Visual route-based navigation for sunny summer days and stormy winter nights. In *Proc. ICRA*, 2012. 1, 2, 6

[47] P. Moulon, P. Monasse, and R. Marlet. Global Fusion of Relative Motions for Robust, Accurate and Scalable Structure from Motion. In *Proc. ICCV*, 2013. 13

[48] P. Moulon, P. Monasse, R. Marlet, and Others. Openmvg. <https://github.com/openMVG/openMVG>. 13

[49] P. Mühlfellner, M. Bürki, M. Bosse, W. Derendarz, R. Philippson, and P. Furgale. Summary maps for lifelong visual localization. *Journal of Field Robotics*, 2015. 2

[50] R. Mur-Artal, J. M. M. Montiel, and J. D. Tards. ORB-SLAM: A Versatile and Accurate Monocular SLAM System. *T-RO*, 31(5):1147–1163, 2015. 2

[51] T. Naseer, G. L. Oliveira, T. Brox, and W. Burgard. Semantics-aware visual localization under challenging perceptual conditions. In *ICRA*, 2017. 1, 2

[52] T. Naseer, L. Spinello, W. Burgard, and C. Stachniss. Robust visual robot localization across seasons using network flows. In *AAAI*, pages 2564–2570, 2014. 6

[53] G. Pandey, J. R. McBride, and R. M. Eustice. Ford campus vision and LIDAR data set. *Intl. J. of Robotics Research*, 30(13):1543–1552, 2011. 3

[54] J. Philbin, O. Chum, M. Isard, J. Sivic, and A. Zisserman. Object retrieval with large vocabularies and fast spatial matching. In *Proc. CVPR*, 2007. 2, 11

[55] R. Pless. Using Many Cameras as One. In *Proc. CVPR*, 2003. 6

[56] F. Radenović, J. L. Schönberger, D. Ji, J.-M. Frahm, O. Chum, and J. Matas. From Dusk till Dawn: Modeling in the Dark. In *Proc. CVPR*, 2016. 2

[57] F. Radenović, G. Tolias, and O. Chum. CNN Image Retrieval Learns from BoW: Unsupervised Fine-Tuning with Hard Examples. In *Proc. ECCV*, 2016. 2

[58] T. Sattler, M. Havlena, F. Radenovic, K. Schindler, and M. Pollefeys. Hyperpoints and fine vocabularies for large-scale location recognition. In *Proc. ICCV*, 2015. 1, 2

[59] T. Sattler, M. Havlena, K. Schindler, and M. Pollefeys. Large-scale location recognition and the geometric burstiness problem. In *Proc. CVPR*, June 2016. 2

[60] T. Sattler, B. Leibe, and L. Kobbelt. Improving Image-Based Localization by Active Correspondence Search. In *Proc. ECCV*, 2012. 1, 2, 6, 11

[61] T. Sattler, B. Leibe, and L. Kobbelt. Efficient & Effective Prioritized Matching for Large-Scale Image-Based Localization. *IEEE PAMI*, 2016. 1, 2, 6, 11

[62] T. Sattler, T. Weyand, B. Leibe, and L. Kobbelt. Image Retrieval for Image-Based Localization Revisited. In *Proc. BMVC*, 2012. 3, 4, 13

[63] J. L. Schönberger and J.-M. Frahm. Structure-From-Motion Revisited. In *Proc. CVPR*, June 2016. 3, 12, 13

[64] J. L. Schönberger, T. Price, T. Sattler, J.-M. Frahm, and M. Pollefeys. A Vote-and-Verify Strategy for Fast Spatial Verification in Image Retrieval. In *Proc. ACCV*, 2016. 13

[65] J. L. Schönberger, F. Radenović, O. Chum, and J.-M. Frahm. From single image query to detailed 3d reconstruction. In *Proc. CVPR*, 2015. 6, 12

[66] J. Shotton, B. Glocker, C. Zach, S. Izadi, A. Criminisi, and A. Fitzgibbon. Scene Coordinate Regression Forests for Camera Relocalization in RGB-D Images. In *Proc. CVPR*, 2013. 2, 3

[67] K. Simonyan and A. Zisserman. Very deep convolutional networks for large-scale image recognition. In *International Conference on Learning Representations*, 2015. 12

[68] J. Sivic and A. Zisserman. Video Google: A text retrieval approach to object matching in videos. In *Proc. ICCV*, 2003. 2

[69] N. Snavely, S. Seitz, and R. Szeliski. Photo Tourism: Exploring Photo Collections in 3D. In *Proc. ACM SIGGRAPH*, 2006. 3

[70] N. Sünderhauf, F. Dayoub, S. Shirazi, B. Upcroft, and M. Milford. On the Performance of ConvNet Features for Place Recognition. In *Proc. IROS*, 2015. 2

[71] N. Sünderhauf, P. Neubert, and P. Protzel. Are we there yet? Challenging SeqSLAM on a 3000 km journey across all four seasons. In *Proc. of Workshop on Long-Term Autonomy, ICRA*, 2013. 3, 6, 12

[72] N. Sünderhauf, S. Shirazi, A. Jacobson, F. Dayoub, E. Peperell, B. Upcroft, and M. Milford. Place Recognition with ConvNet Landmarks: Viewpoint-Robust, Condition-Robust, Training-Free. In *RSS*, 2015. 1, 2

[73] L. Svärm, O. Enqvist, F. Kahl, and M. Oskarsson. City-Scale Localization for Cameras with Known Vertical Direction. *IEEE PAMI*, 2016. 1, 2

[74] A. Teynor and H. Burkhardt. Fast codebook generation by sequential data analysis for object classification. In *International Symposium on Visual Computing*, pages 610–620. Springer, 2007. 11

[75] G. Tolias, Y. S. Avrithis, and H. Jégou. Image search with selective match kernels: Aggregation across single and multiple images. *IJCV*, 116(3):247–261, 2016. 2

[76] A. Torii, R. Arandjelović, J. Sivic, M. Okutomi, and T. Pajdla. 24/7 place recognition by view synthesis. In *Proc. CVPR*, 2015. 1, 2, 11, 12

[77] A. Torii, R. Arandjelović, J. Sivic, M. Okutomi, and T. Pajdla. 24/7 Place Recognition by View Synthesis. In *Proc. CVPR*, 2015. 2, 3, 5

[78] A. Torii, J. Sivic, M. Okutomi, and T. Pajdla. Visual place recognition with repetitive structures. *IEEE PAMI*, 2015. 2

[79] A. Vedaldi and B. Fulkerson. VLFeat - an open and portable library of computer vision algorithms. In *Proc. ACMM*, 2010. 11

[80] F. Walch, C. Hazirbas, L. Leal-Taixé, T. Sattler, S. Hilsenbeck, and D. Cremers. Image-based Localization with Spatial LSTMs. *arXiv:1611.07890*, 2016. 2, 6

[81] T. Weyand, I. Kostrikov, and J. Philbin. Planet - photo geolocation with convolutional neural networks. In *Proc. ECCV*, 2016. 2

[82] C. Wu. Visualsfm: A visual structure from motion system. URL: <http://homes.cs.washington.edu/~ccwu/vsfm>, 9, 2011. 12

[83] C. Wu. Towards Linear-time Incremental Structure From Motion. In *3DV*, 2013. 6

[84] B. Zeisl, T. Sattler, and M. Pollefeys. Camera pose voting for large-scale image-based localization. In *Proc. ICCV*, 2015. 1, 2

## Appendix

This appendix provides additional details and experimental results. Sec. A describes the parameter settings for the reference algorithms used in the paper. Sec. B details the challenges encountered during the reconstruction of the 3D models used for the Aachen Day-Night and the RobotCar Seasons datasets. Sec. C provides the additional experimental results for structure-based localization on the RobotCar Seasons dataset that were mentioned in the paper.

## A. Details on the Reference Algorithms

We provide details, including parameter settings, on the reference algorithms used for experimental evaluation. Following Sec. 4 in the paper, we group the different methods based on common characteristics.

### A.1. 2D Image-based Localization

**FAB-MAP.** For FAB-MAP [18], we trained a separate vocabulary for each location using Modified Sequential Clustering [74] on evenly spaced database images, resulting in 3,585 visual words for Aachen Day-Night and 5,031 for RobotCar Seasons. A Chow-Liu tree was built for each dataset using the Bag-of-Words generated for each database image using the vocabulary. We used the mean field approximation for the new place likelihood (as additional training images were not available for the sampled approach used in [19]) and the fast lookup-table implementation in [24] to perform image retrieval for each of the query locations. Tab. 5 summarizes the parameters used for the experiments.

**DenseVLAD and NetVLAD.** We use the original implementations of DenseVLAD [76] and NetVLAD [2] provided by the authors. We kept an image to have its original size unless the maximum dimension is larger than 1920 pixels. For DenseVLAD, we used the Dense SIFT implementation available in VLFeat [79] followed by RootSIFT normalization [3] and used a visual vocabulary of 128 visual words (centroids) pre-computed on the San-Francisco (SF) dataset [15], *i.e.* we used a general vocabulary trained on a different city dataset. For NetVLAD, we used the pre-computed network “Pitts30k” trained on the Pittsburgh time-machine street-view image dataset [2]. The network is therefore not fine-tuned on our datasets, *i.e.* we again used a general network trained on a different city.

Tables 6 and 7 summarize the parameters used for the experiments.

### A.2. 3D Structure-based Localization

**Active Search.** Active Search [60, 61] uses a visual vocabulary to quantize the descriptor space and bases its prioritized matching scheme on this quantization. For the Aachen Day-Night dataset, we trained a vocabulary containing 100k words using approximate k-means clustering [54] on all upright RootSIFT [3, 39] descriptors found in 1,000 randomly selected database images contained in the 3D model. Similarly, we trained a vocabulary containing 10k words for the RobotCar Seasons dataset from the descriptors found in 1,000 randomly selected images contained in the reference 3D model. Thus, no information from the query images was used to compute the visual vocabularies.

We use calibrated cameras rather than simultaneously estimating each camera’s extrinsic and intrinsic parameters. We thereby exploit the known intrinsic calibrations provided by the base model of the Aachen Day-Night dataset and the known intrinsics of the RobotCar Seasons dataset.

Besides training new vocabularies and using calibrated cameras, we use the standard parameters of Active Search. Thus, Active Search terminates its correspondence search once 100 matches have been found.

**LocalSfM.** For each night-time query image of the Aachen Day-Night dataset, we manually selected a day-time photo taken from a similar viewpoint (*c.f.* Sec. 3.1 in the paper). For each of these equivalent day-time images, we selected the 20 database images contained in the final 3D model that share the largest number of 3D points with it in the base model. For each night-time query, we try to construct a local 3D Structure-from-Motion (SfM) model containing the query and the 20 corresponding database images. To this end, LocalSfM [65] performs exhaustive feature matching between these 21 photos, employing a more relaxed SIFT ratio test threshold [39] of 0.99 to recover more matches<sup>3</sup>. Given the pairwise matches, we use COLMAP [63] to obtain a local SfM model. Using the known positions of the 20 database images in the full 3D model, this local reconstruction is then geo-registered. As a result, the camera pose of the query is obtained if the night-time images was reconstructed.

**DenseSfM.** DenseSfM modifies the LocalSfM approach by replacing RootSIFT [3] features extracted at DoG extrema [39] with features densely extracted from a regular grid [9, 38]. The goal of this approach is to increase the robustness of feature matching between day and night images [76]. We used convolutional layers (conv4 and conv3) from a VGG-16 network [67] which was pre-trained as part of the NetVLAD model (Pitts30k) as features. We generated tentative correspondences by matching the extracted features in a coarse-to-fine manner (first matching conv4 features and using the resulting matches to restrict the correspondence search for the conv3 features). The matches are verified by estimating up to two homographies between each image pair via RANSAC [21]. We performed exhaustive pairwise image matching. The resulting verified feature matches are then used as input for VisualSfM [82] to obtain a local 3D model. As in the LocalSfM, the local reconstruction is geo-registered and the camera pose of the query is reported if the night-time image was reconstructed.

### A.3. Trajectory-based Localization

**3D Structure-based Trajectory.** We use the 3-point-generalized-pose (GP3P) solver from [33] to estimate the pose of each generalized camera (formed either by a triplet of images captured at the same timestamp or temporal sequences of triplets). The matches required for pose estimation are obtained using Active Search on each individual image, *i.e.*, these trajectory-based approaches use the same correspondences as when querying with individual images. As for standard Active Search, a generalized camera is considered as successfully localized if its estimated pose has at least 12 RANSAC inliers.

<sup>3</sup>For comparison, Active Search uses a threshold of 0.7 for 2D-to-3D and a threshold of 0.6 for 3D-to-2D matching.

Parameter	Value
Feature Type	UprightSURF128
Aachen Vocabulary Size	3585
RobotCar Vocabulary Size	5031
$p(z_i   \bar{e}_i)$	0
$p(\bar{z}_i   e_i)$	0.61
$p(L_{\text{new}}   Z^{k-1})$	0.9

Table 5. FAB-MAP parameters.

Parameter	Value
Feature Type	Dense RootSIFT
Vocabulary Size (trained on SF)	128
Descriptor Dimension (after PCA & whitening)	4,096

Table 6. DenseVLAD parameters.

Parameter	Value
Network model (trained on Pitts30k)	VGG-16 + NetVLAD + whitening
Descriptor Dimension	4,096

Table 7. NetVLAD parameters.

Parameter	Value
Image Size	$48 \times 48$ ( $144 \times 48$ )
Patch Size	$8 \times 8$
Sequence Length $d_s$	10

Table 8. SeqSLAM parameters.

In order to use the GP3P solver, the relative poses between the images in a generalized camera, as well as the scale of the camera, need to be known. We observed that local SfM reconstructions using generalized cameras are very accurate over short distances. Rather than computing a local model for each sequence, we thus extract the required relative poses from the ground truth camera poses. Notice that we only use the relative poses and no information about the absolute pose of a generalized camera is used during pose estimation.

**2D Image-based Trajectory.** We used the OpenSeqSLAM implementation in [71] with default parameters for template learning and trajectory uniqueness. For each set of synchronised Grasshopper2 images, we downscale the original  $1024 \times 1024$  resolution to  $48 \times 48$ , then concatenate three images to form a  $144 \times 48$  pixel composite. The trajectory length parameter  $d_s$  was set to 10 images; as both the query and database images are evenly spaced this corresponds to a trajectory length of 10 metres. Tab. 8 summarizes the parameters used for the experiments.

## B. Details on Reconstructing the Datasets

We encountered multiple challenges during the construction of the 3D models for the Aachen Day-Night and RobotCar

Seasons datasets. This section describes these challenges.

**Aachen Day-Night.** Following standard practice for large-scale SfM, we used the image retrieval engine [64] provided by COLMAP [63] for efficient image matching. Fig. 7(left,middle) illustrate intermediate results we obtained with this strategy, in which unrelated parts are merged due to ambiguities in the local features.

In order to avoid these problems, we employed a more careful reconstruction strategy. We obtained an initial model by only matching images that shared 3D points in the original Aachen reconstruction from [62]. Yet, simply adding additional photos using the matches from image retrieval still resulted in a broken model (*c.f.* Fig. 7(middle)). We therefore performed exhaustive feature matching between all images in the incorrect part of the reconstruction and matched these photos against the images already included in the initial model. Finally, we added the images extracted from our newly recorded video sequences to connect previously disconnected parts. Overall, creating the base model took approximately three weeks.

**RobotCar Seasons.** Initial attempts of reconstruction the RobotCar Seasons dataset from the *overcast (reference)* sequence with COLMAP failed as the left-, rear-, and right-facing cameras share no visual overlap. Thus, treating each image independently results in significant drift and severely distorted models. In order to make use of the known extrinsic calibration between the three cameras, we tried a version of the global SfM approach [47] implemented in OpenMVG [48] that is able to handle multi-camera systems. While this resulted in locally consistent reconstructions, we still observed significant drift since parts of the model are only weakly connected.

As a next attempt, we experimented with an iterative approach, implemented on top of COLMAP and using upright RootSIFT [3,39] features. The method initializes all camera poses using the vehicle position reported by the inertial navigation system (INS) mounted on the RobotCar. We then iteratively triangulated 3D points from feature matches, merged tracks, and refined both structure and poses using bundle adjustment [1]. The bundle adjustment procedure enforced consistent relative poses between images taken at the same point in time by the three cameras. Unfortunately, this turned out to be computationally infeasible due to the sheer number of images (more than 20k individual photos) and the dense feature tracks between images taken with the same camera. Thus, we elected to follow the approach of computing non-overlapping local submaps (*c.f.* Sec. 3.2 in the paper). These maps were then registered against the INS poses to obtain a single global model.

## C. Quantitative Results - RobotCar Seasons

This section provides additional detailed experimental results for Active Search on the RobotCar Seasons dataset. These experiments were mentioned in the paper but not included due to space constraints.

**Choice of Camera.** Sec. 5.2 of the paper mentions that more images can be localized using the rear-facing camera compared to the left- and right-facing cameras. Tab. 9 shows the results of the corresponding experiment which evaluates the localization rate and pose accuracy for the three cameras (left-, rear-, and right-facing) mounted on the RobotCar. Looking at the query images shown in the supplementary video, it can be seen that the sideward-facing cameras exhibit motion blur and suffer from overexposure, which is not the case for the rear-facing camera. As a result, the rear-facing camera exhibits a significantly higher localization rate.

Tab. 9 also shows that there is little difference in pose accuracy between the three cameras, *i.e.*, the additional images localized by the rear-facing camera do not come at the price of reduced position and orientation accuracy.

**Pose Accuracy for Structure-based Sequence Localization.** As shown in Tab. 4 in the paper, using all image triplets at all timestamps in a sequence improves the localization rate compared to using a single image and a generalized camera per triplet. Tab. 10 provides the pose accuracy for the three camera setups. A sequence is considered to be localized successfully if at least one image in the sequence has a pose estimate with 12 or more inliers. We measured pose accuracy per sequence by computing the mean pose accuracy for all cameras that have a successful pose estimate. As can be seen, there is little gain in accuracy for the day-time queries when using all image triplets in a sequence for pose estimation. There is a noticeable difference in pose accuracy for the night-time sequences: While using all triplets in a sequence (*full sequence*) increases the localization rate, it also results in reduced pose accuracy. This behavior indicates that only few matches are found for the additionally localized sequences as this is a common cause for inaccurate pose estimates.

To verify this assumption, we performed an additional experiment. By construction of the dataset, each sequence is associated with one of the 49 submaps that form the RobotCar Seasons dataset. Rather than matching features against the 3D points from all submaps, we performed matching only against the corresponding submap. The results of this experiment can be seen in Tab. 11. For reference, Tab. 11 also include the results from Tab. 10 obtained when matching against the full model.

As can be seen, solving a local matching problem results in more correct correspondences and thus a higher localization rate. For the single camera setup, finding more



Figure 7. (left, middle) two broken reconstructions of the Aachen Day-Night dataset obtained without careful matching. In both models, unrelated parts are connected due to local similarities. (right) the final, correct reconstruction (c.f. Fig. 3 in the paper).

condition	camera	loc. rate	Quantile errors: position [m], orientation [°]			
			25%	50%	75%	95%
dawn	left	348 (72.05)	0.20, 0.62	0.30, 0.99	0.51, 1.81	1.19, 4.98
	rear	<b>432 (89.44%)</b>	0.18, 0.40	0.31, 0.61	0.50, 0.93	1.16, 4.75
	right	393 (81.37)	0.18, 0.45	0.31, 0.70	0.54, 1.21	1.31, 4.70
dusk	left	362 (91.88)	0.17, 0.96	0.29, 1.23	0.48, 1.80	1.11, 4.44
	rear	<b>378 (95.94%)</b>	0.18, 0.64	0.26, 0.78	0.41, 0.96	1.02, 4.25
	right	330 (83.76)	0.21, 0.78	0.31, 0.98	0.50, 1.27	0.98, 4.28
night	left	3 (0.68)	0.48, 1.58	0.55, 2.08	0.80, 5.58	1.00, 8.39
	rear	<b>15 (3.42%)</b>	0.49, 0.74	0.61, 0.94	0.81, 3.36	0.96, 6.05
	right	10 (2.28)	0.47, 0.57	0.69, 1.05	1.05, 1.43	1.28, 2.07
night+rain	left	16 (3.64)	0.45, 1.15	0.59, 2.02	1.18, 4.22	1.48, 6.43
	rear	<b>19 (4.32%)</b>	0.26, 0.58	0.33, 0.69	0.41, 1.08	1.42, 1.56
	right	0 (0%)	-	-	-	-
overcast (summer)	left	366 (79.05)	0.26, 1.03	0.38, 1.45	0.70, 2.07	1.14, 4.30
	rear	<b>442 (95.46%)</b>	0.24, 0.84	0.36, 1.06	0.59, 1.45	1.09, 4.14
	right	405 (87.47)	0.22, 0.79	0.33, 0.99	0.63, 1.36	1.15, 4.26
overcast (winter)	left	318 (81.54)	0.22, 1.16	0.32, 1.49	0.59, 2.10	1.35, 4.26
	rear	<b>365 (93.59%)</b>	0.21, 0.68	0.32, 0.89	0.45, 1.20	1.25, 4.10
	right	314 (80.51)	0.24, 0.88	0.35, 1.13	0.59, 1.56	1.13, 4.46
rain	left	404 (95.96)	0.18, 0.49	0.26, 0.72	0.42, 1.16	1.00, 4.19
	rear	<b>409 (97.15%)</b>	0.15, 0.73	0.24, 0.90	0.42, 1.11	0.94, 4.96
	right	395 (93.82)	0.22, 0.55	0.31, 0.79	0.46, 1.21	0.96, 4.65
snow	left	376 (76.89)	0.17, 1.00	0.28, 1.31	0.42, 1.80	1.15, 4.22
	rear	<b>455 (93.05%)</b>	0.18, 0.57	0.29, 0.78	0.44, 1.16	1.14, 4.20
	right	400 (81.80)	0.18, 0.83	0.30, 1.04	0.46, 1.49	1.19, 4.35
sun	left	178 (38.70)	0.21, 0.80	0.38, 1.23	0.76, 1.98	1.50, 4.41
	rear	<b>314 (68.26%)</b>	0.20, 0.74	0.33, 1.01	0.57, 1.45	1.30, 4.15
	right	242 (52.61)	0.19, 0.84	0.35, 1.04	0.53, 1.44	1.14, 4.51

Table 9. The impact of using **different cameras** for the **RobotCar Seasons dataset**: We report the localization rate as the number and percentage of localized queries as well as the quantiles on the pose errors. As can be seen, a higher localization rate can be achieved with the rear camera compared to the other two cameras. At the same time, the choice of camera has little impact on the pose accuracy.

matches also results in a higher pose accuracy, *i.e.*, we can again observe that the single camera setup either localizes a night-time query rather accurately or not at all. As for the *full sequence* setup in the previous experiment, the pose accuracy of the *generalized* setup decreases while additional sequences are localized. In contrast, the localization rate of the *full sequence* setup increases while its pose accuracy increases as well. This demonstrates that the previ-

ous decrease in accuracy was caused by finding just enough matches for localizing additional images but not enough for accurate pose estimation.

The results of this last experiment suggest that local matching is preferable. This behavior was already shown on the Aachen Day-Night dataset as the two methods based on local SfM reconstruction (*LocalSfM* and *DenseSfM*) outperformed Active Search.

condition	# sequences	camera setup	loc. rate	Quantile errors: position [m], orientation [°]			
				25%	50%	75%	95%
all day	360	single generalized full sequence	334 (92.8%)	0.22, 0.74	0.34, 0.91	0.49, 1.24	1.11, 4.42
			342 (95%)	0.18, 0.62	0.25, 0.76	0.40, 0.94	1.00, 4.33
			346 (96.11%)	0.15, 0.57	0.23, 0.78	0.39, 1.02	1.02, 4.36
all night	100	single generalized full sequence	9 (9%)	0.33, 0.70	0.47, 1.28	0.78, 1.34	1.03, 4.54
			24 (24%)	0.29, 0.63	0.44, 0.97	0.85, 2.66	1.42, 5.56
			41 (41%)	0.28, 0.65	0.74, 1.18	1.17, 4.98	3.72, 17.15

Table 10. Localization rate and pose accuracy for **localizing sequences** on the **RobotCar Seasons** dataset: We report results for using a single rear-facing camera per timestamp (*single*), image triplets per timestamp (*generalized*), and using all triplets in the sequence (*full sequence*). For each camera setup, we report the localization rate and the quantiles on the pose errors.

condition	# sequences	camera setup	matched against	loc. rate	Quantile errors: position [m], orientation [°]			
					25%	50%	75%	95%
all night	100	single	full model	9 (9%)	0.33, 0.70	0.47, 1.28	0.78, 1.34	1.03, 4.54
			submap	21 (21%)	0.29, 0.58	0.38, 0.78	0.55, 1.11	1.14, 4.52
		generalized	full model	24 (24%)	0.29, 0.63	0.44, 0.97	0.85, 2.66	1.42, 5.56
			submap	38 (38%)	0.31, 0.60	0.52, 1.05	0.90, 2.01	2.45, 6.06
		full sequence	full model	41 (41%)	0.28, 0.65	0.74, 1.18	1.17, 4.98	3.72, 17.15
			submap	65 (65%)	0.27, 0.63	0.43, 0.93	0.76, 1.85	1.47, 5.29

Table 11. Localization rate and pose accuracy for **localizing sequences** on the **RobotCar Seasons** dataset against **individual submaps**: We report results for using a single rear-facing camera per timestamp (*single*), image triplets per timestamp (*generalized*), and using all triplets in the sequence (*full sequence*). For each camera setup, we report the localization rate and the quantiles on the pose errors. We compare the localization performance obtained when matching each (generalized) camera or sequence against the *full model* containing all submaps and when matching against the submap containing the (generalized) camera or sequence (*submap*).